# A comparative study on chirped-pulse upconversion and direct multichannel MCT detection

**Johannes Knorr, Philipp Rudolf, and Patrick Nuernberger***

*Institut für Physikalische und Theoretische Chemie, Universität Würzburg, Am Hubland, 97074 Würzburg, Germany*

*nuernberger@phys-chemie.uni-wuerzburg.de

**Abstract:** A comparative study is carried out on two spectroscopic techniques employed to detect ultrafast absorption changes in the mid-infrared spectral range, namely direct multichannel detection via HgCdTe (MCT) photodiode arrays and the newly established technique of chirped-pulse upconversion (CPU). Whereas both methods are meanwhile individually used in a routine manner, we directly juxtapose their applicability in femtosecond pump-probe experiments based on 1 kHz shot-to-shot data acquisition. Additionally, we examine different phase-matching conditions in the CPU scheme for a given mid-infrared spectrum, thereby simultaneously detecting signals which are separated by more than 200 $cm^{-1}$.



**OCIS codes:** (320.7150) Ultrafast spectroscopy; (190.7220) Upconversion; (300.6340) Spectroscopy, infrared; (160.3730) Lithium niobate; (040.1520) CCD, charge-coupled device.

## References and links

1. P. Stoutland, R. Dyer, and W. Woodruff, "Ultrafast infrared spectroscopy," Science **257**, 1913–1917 (1992).
2. P. Hamm, S. Wiemann, M. Zurek, and W. Zinth, "Highly sensitive multichannel spectrometer for subpicosecond spectroscopy in the midinfrared," Opt. Lett. **19**, 1642–1644 (1994).
3. P. Hamm, R. A. Kaindl, and J. Stenger, "Noise suppression in femtosecond mid-infrared light sources," Opt. Lett. **25**, 1798–1800 (2000).
4. G. Cerullo and S. D. Silvestri, "Ultrafast optical parametric amplifiers," Rev. Sci. Instrum. **74**, 1–18 (2003).
5. J. Moore, P. Hansen, and R. Hochstrasser, "A new method for picosecond time-resolved infrared spectroscopy: applications to CO photodissociation from iron porphyrins," Chem. Phys. Letters **138**, 110–114 (1987).
6. T. P. Dougherty and E. J. Heilweil, "Dual-beam subpicosecond broadband infrared spectrometer," Opt. Lett. **19**, 129–131 (1994).
7. M. Lim, T. Jackson, and P. Anfinrud, "Binding of CO to myoglobin from a heme pocket docking site to form nearly linear Fe-C-O," Science **269**, 962–966 (1995).
8. I. V. Rubtsov, T. Zhang, H. Nakajima, S. Aono, G. I. Rubtsov, S. Kumazaki, and K. Yoshihara, "Conformational dynamics of the transcriptional regulator CooA protein studied by subpicosecond mid-infrared vibrational spectroscopy," J. Am. Chem. Soc. **123**, 10056–10062 (2001).
9. J. Herbst, K. Heyne, and R. Diller, "Femtosecond infrared spectroscopy of bacteriorhodopsin chromophore isomerization," Science **297**, 822–825 (2002).
10. H. J. Bakker, H.-K. Nienhuys, G. Gallot, N. Lascoux, G. M. Gale, J.-C. Leicknam, and S. Bratos, "Transient absorption of vibrationally excited water," J. Chem. Phys. **116**, 2592–2598 (2002).
11. E. T. J. Nibbering and T. Elsaesser, "Ultrafast vibrational dynamics of hydrogen bonds in the condensed phase," Chem. Rev. **104**, 1887–1914 (2004).
12. J. Bredenbeck, J. Helbing, J. R. Kumita, G. A. Woolley, and P. Hamm, "$\alpha$-Helix formation in a photoswitchable peptide tracked from picoseconds to microseconds by time-resolved IR spectroscopy," Proc. Natl. Acad. Sci. U.S.A. **102**, 2379–2384 (2005).
13. M. L. Groot, L. J. G. W. van Wilderen, and M. Di Donato, "Time-resolved methods in biophysics. 5. Femtosecond time-resolved and dispersed infrared spectroscopy on proteins," Photochem. Photobiol. Sci. **6**, 501–507 (2007).

#199085 - $15.00 USD Received 7 Oct 2013; revised 11 Nov 2013; accepted 11 Nov 2013; published 5 Dec 2013

14. W. J. Schreier, T. E. Schrader, F. O. Koller, P. Gilch, C. E. Crespo-Hernández, V. N. Swaminathan, T. Carell, W. Zinth, and B. Kohler, "Thymine dimerization in DNA is an ultrafast photoreaction," Science **315**, 625–629 (2007).
15. J. Treuffet, K. J. Kubarych, J.-C. Lambry, E. Pilet, J.-B. Masson, J.-L. Martin, M. H. Vos, M. Joffre, and A. Alexandrou, "Direct observation of ligand transfer and bond formation in cytochrome c oxidase by using mid-infrared chirped-pulse upconversion," Proc. Natl. Acad. Sci. U.S.A **104**, 15705–15710 (2007).
16. D. Cringus, A. Bakulin, J. Lindner, P. Vöhringer, M. S. Pshenichnikov, and D. A. Wiersma, "Ultrafast energy transfer in water-AOT reverse micelles," J. Phys. Chem. B **111**, 14193–14207 (2007).
17. Y. Zhang, G. Burdzinski, J. Kubicki, and M. S. Platz, "Direct observation of carbene and diazo formation from aryldiazirines by ultrafast infrared spectroscopy," J. Am. Chem. Soc. **130**, 16134–16135 (2008).
18. P. Rudolf, J. Buback, J. Aulbach, P. Nuernberger, and T. Brixner, "Ultrafast multisequential photochemistry of 5-diazo Meldrum's acid," J. Am. Chem. Soc. **132**, 15213–15222 (2010).
19. S. Yan, M. T. Seidel, Z. Zhang, W. K. Leong, and H.-S. Tan, "Ultrafast vibrational relaxation dynamics of carbonyl stretching modes in $Os_3(CO)_{12}$," J. Chem. Phys. **135**, 024501 (2011).
20. P. Nuernberger, K. F. Lee, A. Bonvalet, L. Bouzhir-Sima, J.-C. Lambry, U. Liebl, M. Joffre, and M. H. Vos, "Strong ligand-protein interactions revealed by ultrafast infrared spectroscopy of CO in the heme pocket of the oxygen sensor FixL," J. Am. Chem. Soc. **133**, 17110–17113 (2011).
21. Y. Yang, M. Linke, T. von Haimberger, J. Hahn, R. Matute, L. González, P. Schmieder, and K. Heyne, "Real-time tracking of phytochrome's orientational changes during Pr photoisomerization," J. Am. Chem. Soc. **134**, 1408–1411 (2012).
22. J. P. Lomont, S. C. Nguyen, and C. B. Harris, "Ultrafast TRIR and DFT studies of the photochemical dynamics of $Co_4(CO)_{12}$ in solution," Organometallics **31**, 4031–4038 (2012).
23. A. Lukacs, R.-K. Zhao, A. Haigney, R. Brust, G. M. Greetham, M. Towrie, P. J. Tonge, and S. R. Meech, "Excited state structure and dynamics of the neutral and anionic flavin radical revealed by ultrafast transient mid-IR to visible spectroscopy," J. Phys. Chem. B **116**, 5810–5818 (2012).
24. P. Rudolf, F. Kanal, J. Knorr, C. Nagel, J. Niesel, T. Brixner, U. Schatzschneider, and P. Nuernberger, "Ultrafast photochemistry of a manganese-tricarbonyl CO-releasing molecule (CORM) in aqueous solution," J. Phys. Chem. Lett. **4**, 596–602 (2013).
25. N. T. Hunt, "2D-IR spectroscopy: ultrafast insights into biomolecule structure and function," Chem. Soc. Rev. **38**, 1837–1848 (2009).
26. K. J. Kubarych, M. Joffre, A. Moore, N. Belabas, and D. M. Jonas, "Mid-infrared electric field characterization using a visible charge-coupled-device-based spectrometer," Opt. Lett. **30**, 1228–1230 (2005).
27. M. J. Nee, R. McCanne, K. J. Kubarych, and M. Joffre, "Two-dimensional infrared spectroscopy detected by chirped pulse upconversion," Opt. Lett. **32**, 713–715 (2007).
28. P. Nuernberger, K. F. Lee, A. Bonvalet, M. H. Vos, and M. Joffre, "Multiply excited vibration of carbon monoxide in the primary docking site of hemoglobin following photolysis from the heme," J. Phys. Chem. Lett. **1**, 2077–2081 (2010).
29. J. M. Anna, M. J. Nee, C. R. Baiz, R. McCanne, and K. J. Kubarych, "Measuring absorptive two-dimensional infrared spectra using chirped-pulse upconversion detection," J. Opt. Soc. Am. B **27**, 382–393 (2010).
30. R. Maksimenka, P. Nuernberger, K. F. Lee, A. Bonvalet, J. Milkiewicz, C. Barta, M. Klima, T. Oksenhendler, P. Tournois, D. Kaplan, and M. Joffre, "Direct mid-infrared femtosecond pulse shaping with a calomel acousto-optic programmable dispersive filter," Opt. Lett. **35**, 3565–3567 (2010).
31. K. F. Lee, P. Nuernberger, A. Bonvalet, and M. Joffre, "Removing cross-phase modulation from midinfrared chirped-pulse upconversion spectra," Opt. Express **17**, 18738–18744 (2009).
32. J. Zhu, T. Mathes, A. D. Stahl, J. T. Kennis, and M. L. Groot, "Ultrafast mid-infrared spectroscopy by chirped pulse upconversion in 1800-1000 $cm^{-1}$ region," Opt. Express **20**, 10562–10571 (2012).
33. C. R. Baiz and K. J. Kubarych, "Ultrabroadband detection of a mid-IR continuum by chirped-pulse upconversion," Opt. Lett. **36**, 187–189 (2011).
34. Y. Nomura, Y.-T. Wang, T. Kozai, H. Shirai, A. Yabushita, C.-W. Luo, S. Nakanishi, and T. Fuji, "Single-shot detection of mid-infrared spectra by chirped-pulse upconversion with four-wave difference frequency generation in gases," Opt. Express **21**, 18249–18254 (2013).
35. W. Rock, Y.-L. Li, P. Pagano, and C. M. Cheatum, "2D IR spectroscopy using four-wave mixing, pulse shaping, and IR upconversion: A quantitative comparison," J. Phys. Chem. A **117**, 6073–6083 (2013).
36. P. Nuernberger, G. Vogt, R. Selle, S. Fechner, T. Brixner, and G. Gerber, "Generation of shaped ultraviolet pulses at the third harmonic of titanium-sapphire femtosecond laser radiation," Appl. Phys. B **88**, 519–526 (2007).
37. N. Jacquinet-Husson, N.A. Scott, A. Chédin, L. Crépeau, R. Armante, V. Capelle, J. Orphal, A. Coustenis, C. Boonne, N. Poulet-Crovisier, A. Barbe, M. Birk, L.R. Brown, C. Camy-Peyret, C. Claveau, K. Chance, N. Christidis, C. Clerbaux, P.F. Coheur, V. Dana, L. Daumont, M.R. De Backer-Barilly, G. Di Lonardo, J.M. Flaud, A. Goldman, A. Hamdouni, M. Hess, M.D. Hurley, D. Jacquemart, I. Kleiner, P. Köpke, J.Y. Mandin, S. Massie, S. Mikhailenko, V. Nemtchinov, A. Nikitin, D. Newnham, A. Perrin, V.I. Perevalov, S. Pinnock, L. Régalia-Jarlot, C.P. Rinsland, A. Rublev, F. Schreier, L. Schult, K.M. Smith, S.A. Tashkun, J.L. Teffo, R.A. Toth, VI.G. Tyuterev, J. Vander Auwera, P. Varanasi, and G. Wagner, "The GEISA spectroscopic database:

#199085 - $15.00 USD Received 7 Oct 2013; revised 11 Nov 2013; accepted 11 Nov 2013; published 5 Dec 2013

Current and future archive for earth and planetary atmosphere studies," J. Quant. Spectrosc. Radiat. Transf. **109**, 1043–1059 (2008).
38. M. Kaucikas, J. Barber, and J. J. van Thor, "Polarization sensitive ultrafast mid-IR pump probe microspectrometer with diffraction limited spatial resolution," Opt. Express **21**, 8357–8370 (2013).
39. R. W. Boyd, *Nonlinear Optics* (Academic Press, 2008).
40. D. E. Zelmon, D. L. Small, and D. Jundt, "Infrared corrected Sellmeier coefficients for congruently grown lithium niobate and 5 mol.% magnesium oxide –doped lithium niobate," J. Opt. Soc. Am. B **14**, 3319–3322 (1997).

## 1. Introduction

Revealing the vibrational dynamics of molecules by mapping their transient absorption in the mid-infrared (MIR) spectral range is commonly used to gain insight into chemical processes on a microscopic scale [1]. Over the last decades the development of commercially available amplified femtosecond laser systems, accompanied by the establishment of optical parametric amplifiers capable of generating stable ultrashort MIR pulses [2–4], gave rise to a vast variety of time-resolved investigations on diverse systems in the liquid phase, ranging from small molecules via organometallic compounds to large proteins [5–24].

Standard direct multichannel MIR detection uses liquid nitrogen cooled photodiode arrays based on compound semiconductors as InAs, InSb, or HgCdTe (MCT). Commercially available IR spectrometers are limited to a maximum of 128 pixels, so that combining detector arrays is one way to increase the number of detection channels [23, 25]. Nevertheless, often a compromise between spectral resolution and spectral bandwidth has to be found. Different techniques have been reported, circumventing this issue by transferring the MIR signals to the visible regime [5, 6]. The technique of chirped-pulse upconversion (CPU) in particular uses a strongly chirped near-infrared pulse (CP) to upconvert the characteristic infrared absorption via sum-frequency mixing in a nonlinear crystal [26]. As a result, mature silicon CCD technology can be used to detect the upconverted radiation. Meanwhile, CPU has become a well-established technique in the field of ultrafast MIR spectroscopy [15,20,27–29] and pulse characterization [26, 30]. The possibility to remove cross-phase modulation, introduced by the time-dependent phase of the CP, from upconverted spectra by means of a robust Fourier-transform-based algorithm radically improved the spectral resolution of CPU [31] and thus extended the range of possible applications. For instance, CPU has been applied in the lower energetic regime of 1000-1800 $cm^{-1}$ by using a $AgGaGeS_4$ crystal [32] or to detect ultrabroad MIR continua [33]. Alternatively, CPU was used for upconversion of a MIR supercontinuum spanning from 200 to 5500 $cm^{-1}$ by replacing the upconversion crystal by gas media; apart from a reduced upconversion efficiency, an almost unlimited upconversion bandwidth has been reported [34].

Very recently, Cheatum and coworkers [35] published a comparative study, examining the detection of 2D IR spectra based on a pulse-shaping apparatus, using direct singlechannel MCT detection and visible multichannel detection via a CMOS array, respectively. Unlike in CPU, bandwidth-narrowed 800 nm light was used for upconversion of the MIR pulses. With reference to their results, we compare direct multichannel detection with an MCT array and multichannel detection with a CCD camera after upconversion with a strongly chirped NIR pulse. The goal of the present study is to determine which method is better suited to detect weak absorption-change signals on the order of a mOD or below with respect to the accessible spectral bandwidth, the spectral sampling, and the respective noise levels. Thereby, significant emphasis has been put on an experimental configuration that ensures a high degree of comparability. In the second part of the paper, we examine different phase-matching conditions in the CPU scheme by varying the angle between the incident beams and the optical axis of the nonlinear crystal. We thereby elucidate the possibility to optimize the shape of the CPU spectrum with respect to the detection range of the visible detector.

#199085 - $15.00 USD Received 7 Oct 2013; revised 11 Nov 2013; accepted 11 Nov 2013; published 5 Dec 2013

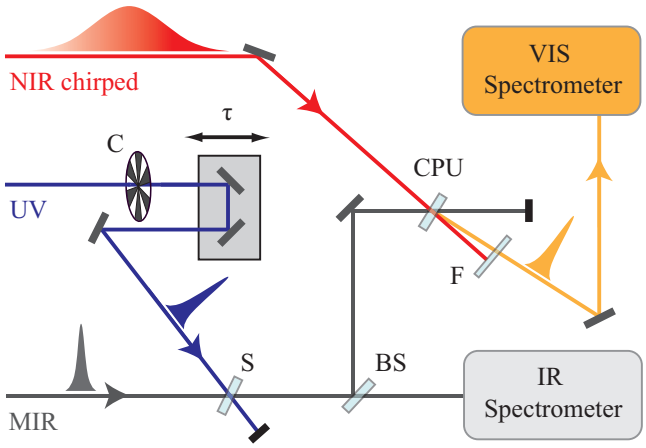


Fig. 1. Schematic illustration of the experimental setup: CPU, upconversion of MIR pulses via sum-frequency mixing with strongly chirped NIR pulses in a $MgO:LiNbO_3$ crystal; F, 750 nm shortpass filter; BS, 50/50 MIR beam splitter; S, sample in flow cell; $\tau$: translation stage to adjust the UV-pump/MIR-probe delay; C, mechanical chopper. Several mirrors and lenses are not sketched for clarity.

## 2. Experimental setup

In the following, the experimental setup is described in detail, whereby the crucial parts of the comparative study are depicted in Fig. 1. All radiation originates from a 1 kHz Ti:Sapphire regenerative amplifier system (Solstice - Spectra-Physics) generating sub 100 fs pulses at a central wavelength of 800 nm. A small portion of the output power is split off and sent through the grating pulse compressor of another available chirped pulse amplification laser system to produce the CP required for upconversion. As a result, we use a downchirped NIR pulse, in contrast to other implementations reported in the literature [15]. The main part of the fundamental beam is used in a noncollinear optical parametric amplifier (NOPA, TOPAS-White - Light Conversion Ltd) to generate 270 nm UV pump pulses. Tunable MIR probe pulses stem from a home-built two-stage optical parametric amplifier (OPA) with subsequent difference-frequency generation (for design details see [3]), pumped by the NOPA residual 800 nm beam. For pump-probe experiments, the 800 nJ UV pulses and the MIR pulses are spatially overlapped in a flow cell providing a 100 μm liquid film between 4 mm $CaF_2$ windows, whereas the time delay is controlled by a linear translation stage. For shot-to-shot data acquisition of absorption-change signals, a mechanical chopper is used to block every second pump pulse. Additionally, the influence of water vapor absorption can be reduced by purging the housings, which encapsulate the main part of the optical MIR paths, with dry air. The polarization directions are chosen in the magic angle configuration (54.7°) to exclude effects attributable to rotational diffusion. After passing the sample the MIR beam is equally split by a KBr window. One half of the probe beam is dispersed by a 150 grooves/mm grating (4.0 μm blaze wavelength) in an IR spectrograph (250 is/sm - Chromex, 4.9 μm central calibration wavelength) and detected by a 32 element MCT-array (InfraRed Associates, Inc.), which can be read out for each laser shot, resulting in a bandwidth of 10.2 nm (corresponding to 4.2 $cm^{-1}$ at the given central wavelength) per pixel. The second half of the probe beam gets upconverted to the visible regime: for this, the MIR signal (pulse energies of several hundred nJ), focussed by a 90° off-axis parabolic mirror (152 mm effective focal length), is mixed with the 18 μJ chirped NIR pulse (centered at 12538 $cm^{-1}$, FWHM 143 $cm^{-1}$) in a noncollinear sum-frequency generation (SFG) arrangement ($\approx 7°$) us-

#199085 - $15.00 USD Received 7 Oct 2013; revised 11 Nov 2013; accepted 11 Nov 2013; published 5 Dec 2013

ing a MgO(5%):$LiNbO_3$ crystal (10 x 10 $mm^2$ x 0.45 mm, type I, 45.4° cut - Castech Inc.). For fine-tuning, we rotate the crystal mount in order to change the angle between the incident beams and the optical axis of the crystal in a well-defined way. The residual CP is rejected by a 750 nm shortpass filter and a 15 cm lens is used to recollimate the CPU signal. A visible 50 cm focal length spectrograph (Acton SpectraPro 2500i - Princeton Instruments, 690 nm central calibration wavelength) equipped with a 1200 grooves/mm grating (750 nm blaze wavelength) in combination with a thermoelectrically cooled 2048 x 512 pixel front-illuminated CCD camera (PIXIS - Princeton Instruments) provides a bandwidth of 0.019 nm (corresponding to 0.40 $cm^{-1}$ at the given central wavelength) per pixel in the range between 670 and 709 nm. For low-speed measurements, 20 pixels are vertically binned and averaged over 300 ms. An additional binning of pairs of adjacent horizontal pixels enables single-shot data acquisition of single-line spectra of 1024 pixels (0.038 nm bandwidth per data point, corresponding to 0.80 $cm^{-1}$ at the given central wavelength). For each spectrum, cross-phase modulations are removed [31] and replicas at 6.8 ps, due to reflections in the upconversion crystal, are Fourier-filtered in the time domain in an area of 1 ps. Being the main spectral phase contribution of the CP, the second-order spectral phase parameter [36] was determined by frequency-resolved cross correlation to be $\phi_2 = -3.97\ ps^2$.

## 3. Accordance of spectra and noise analysis

The first part of the comparative study is carried out using the spectra shown in Fig. 2. In order to get a detailed picture of the MIR spectrum on the one hand, and not being restricted to 32 pixels in the direct MCT detection, we scan the central spectrometer wavelength in steps of 1 nm and detect the signal with the central pixel of the MCT array (blue). On the other hand, we record the upconverted spectrum with the VIS spectrometer. Thus, we obtain approximately the same spectral increment with both detection methods. Whereas the MCT measurement requires a few

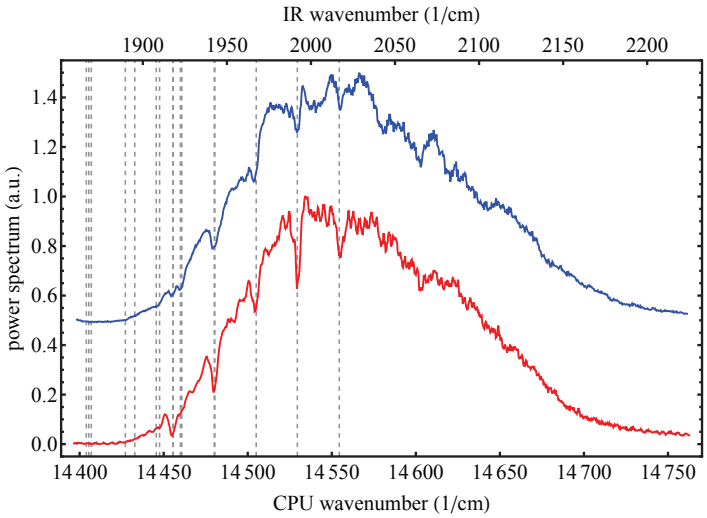


Fig. 2. MIR spectrum obtained with a single HgCdTe pixel by scanning the central IR spectrometer wavelength in steps of 1 nm (blue, centered at 2028 $cm^{-1}$, FWHM 154 $cm^{-1}$, 100 laser shots averaged per step, 5 min total measurement time); MIR spectrum after upconversion and chirp correction detected via CCD camera (red, centered at 14554 $cm^{-1}$, FWHM 151 $cm^{-1}$, 300 ms exposure time); the frequencies of the 16 most intense water vapor lines taken from the GEISA database [37] are depicted as gridlines.

#199085 - $15.00 USD Received 7 Oct 2013; revised 11 Nov 2013; accepted 11 Nov 2013; published 5 Dec 2013

minutes of acquisition time, we obtain the corresponding CPU spectrum in less than one second of exposure (red). In contrast to measurements in the single-shot mode, we use spectrometer slit widths as small as possible and do not flood the housings with dry air, in order to resolve distinct water vapor absorption lines convenient for calibration of the upconversion frequency. Note that the stronger water vapor absorption in the CPU spectrum is due to a longer optical MIR path through water vapor in our laboratory atmosphere. Owing to the crystals phase-matching capabilities, which are examined in greater detail in the second part of this paper, the MIR spectrum (FWHM 154 $cm^{-1}$) gets upconverted to the visible regime with a rather small narrowing of only 3 $cm^{-1}$ of spectral bandwidth.

To analyze the investigated detection methods when detecting ultrafast absorption changes, we choose a 5 mM solution of $Co_4(CO)_{12}$ (Strem Chemicals, Inc.) dissolved in $CH_2Cl_2$ as model system in all experiments of this study. Harris and coworkers [22] found that this molecule undergoes two photochemical reaction pathways when being excited at 267 or 400 nm: besides the formation of CO-loss products arising from the dissociation of a single carbonyl ligand from the parent molecule, two rearrangement isomers are formed. These bridged intermediates, originating from cleavage of an apical-basal Co-Co bond, showed picosecond lifetimes. The compound was considered to be appropriate to be employed in our comparison study owing to its rich photochemistry between 1800 and 2100 $cm^{-1}$ and its high stability in dilute solutions.

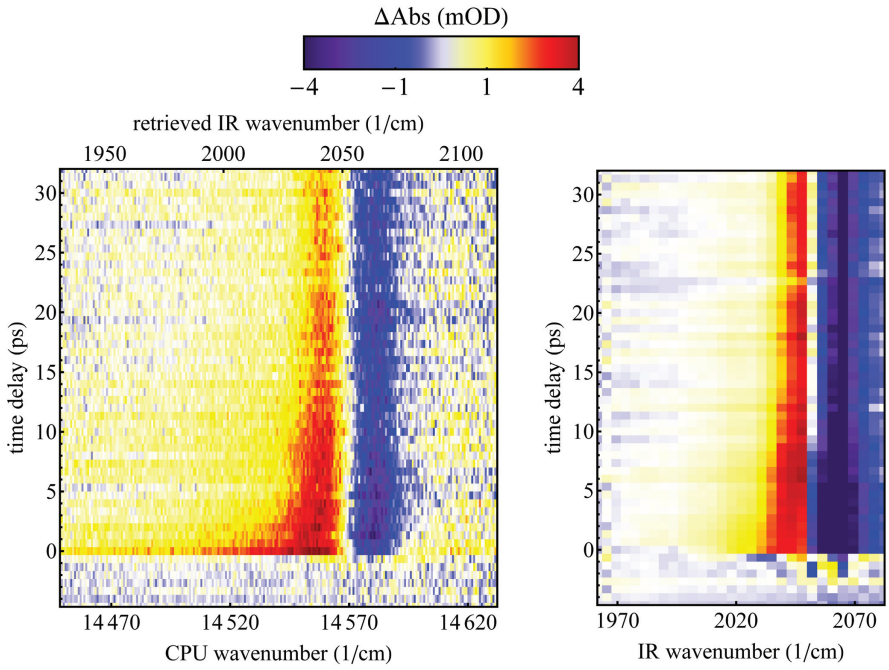


Fig. 3. Transient absorption of $Co_4(CO)_{12}$ under 270 nm UV excitation: data is obtained via CPU (left) and multichannel MCT detection (right), respectively. For each time step 1000 pump-probe pairs are consecutively recorded with each detection method. No data interpolation was used in both graphics.

To gain an overview of the photochemical rearrangement dynamics of our molecular model system and to get a first impression of the capabilities of both detection methods, Fig. 3 displays the transient absorption of $Co_4(CO)_{12}$ for pump-probe time delays up to 32 ps. Deviant from

#199085 - $15.00 USD Received 7 Oct 2013; revised 11 Nov 2013; accepted 11 Nov 2013; published 5 Dec 2013

the default setting, the central wavelength of the IR spectrometer was set to 4.95 μm in this particular measurement. The observed ground-state-bleach signals of the parent compound as well as the positive absorption of upcoming photoproducts at lower energies are in agreement with the literature [22]. Note that each transient absorption spectrum displays the average of only 1000 consecutively measured pump-probe pairs, already providing convincing data qualities. In the following, we will have a closer look at data points of a single transient absorption spectrum, in order to analyze the spectral sampling and the respective noise levels of both detection methods.

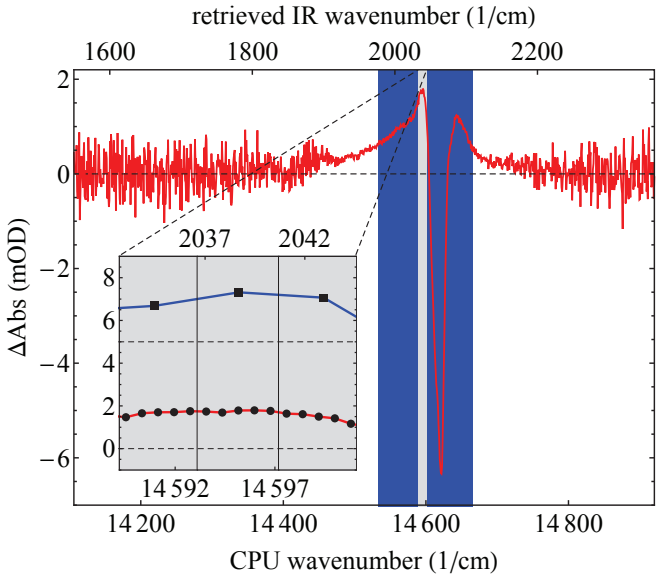


Fig. 4. Transient absorption spectrum of $Co_4(CO)_{12}$ at 6 ps pump-probe delay under 270 nm UV excitation: data obtained by averaging 25000 consecutive pump-probe pairs using CPU detection (red); the blue-shaded area illustrates the full detection range of direct MIR detection; the inset depicts the spectral increment of both detection methods: data points of direct MIR detection via MCT array (blue) are shown with 5 mOD vertical offset; vertical lines confine data points which are used for analysis of individual noise levels (confer Figs. 5 and 6).

Using the laser settings with corresponding spectra from Fig. 2 at a slightly different upconversion frequency, we perform analysis of 50000 transient absorption spectra recorded with both spectrometers in the single-shot acquisition mode. We cannot read out both spectrometers for each laser shot simultaneously. Nevertheless, aiming at a high comparability, we use a measurement routine in which we record 50 loops of a sequence containing subsequent data acquisition of 2000 spectra with each spectrometer as well as data processing. Thereby, the influence of long-term laser fluctuations is minimized. Within two separate runs of the measurement routine under unaltered experimental conditions, we examine the detection of spectra without a molecular signal, which corresponds to the baseline when calculating changes in optical density, as well as the influence of the liquid sample film between the windows in combination with a UV-pump interaction. Absorption-change signals are calculated from consecutive background-corrected spectra followed by averaging. As depicted in Fig. 4, the resulting transient absorption spectrum from the measurement with sample and pump-interaction after averaging over 25000 transient absorption spectra at 6 ps pump-probe delay using CPU detec-

#199085 - $15.00 USD Received 7 Oct 2013; revised 11 Nov 2013; accepted 11 Nov 2013; published 5 Dec 2013

tion (red) illustrates the large detection range of the latter technique: in our case, CPU detection covers more than 200 $cm^{-1}$, only being restricted to the bandwidth of the upconverted spectrum, whereas the MCT detection is limited to approximately 130 $cm^{-1}$ with the employed grating (indicated by the blue-shaded area). For MCT detection in a broader range, one has to change the grating position and repeat the measurement procedure. Especially in time-critical measurements, e.g. when samples tend to degenerate, this constitutes a significant disadvantage. Note that slightly different experimental settings result in minor deviations in the absolute values of changes in optical density with respect to Fig. 3. The individual data points in the inset of Fig. 4 illustrate the different spectral sampling. With respect to the direct MCT detection, the latter is increased by a factor five using CPU. We want to stress that these values reflect a particular experimental situation. Using different grating settings or different array sizes, either the spectral bandwidth or the spectral sampling can be favored. Nevertheless, the higher flexibility of CPU detection is evident.

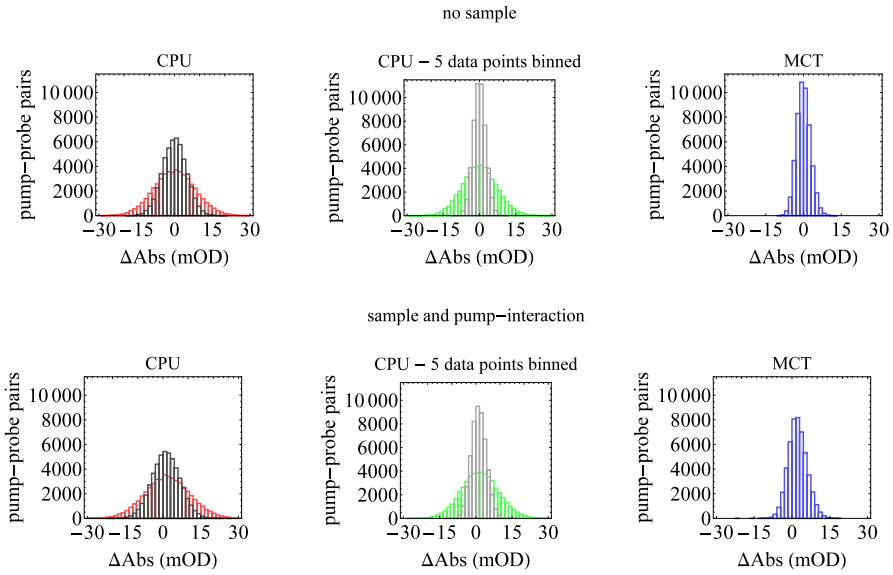


Fig. 5. Histograms illustrating the distribution of 50000 consecutively measured pump-probe pairs for the detection of the signal baseline (top row, no sample) and the detection of a molecular signal of $\Delta Abs \approx 2$ mOD at 2039 $cm^{-1}$ (bottom row, sample and pump-interaction). Besides the histograms for CPU detection (left panels, red) and MCT detection (right panels, blue), representing a single data point, the results for an additional binning of five adjacent CPU data points are shown (middle panels, green). Distributions resulting after normalization of individual spectra with their integrated spectral intensity are shown for CPU detection (left panels, black) and CPU detection with an additional binning of five adjacent data points (middle panels, gray).

For noise analysis, we have a closer look at a single data point at 2039 $cm^{-1}$, which corresponds in the measurement with sample and pump-interaction to a positive absorption-change signal of $\approx 2$ mOD, reflecting overlapping terminal carbonyl stretches of transient photoproducts. The histograms in Fig. 5 illustrate the Gaussian distribution of 50000 consecutively measured pump-probe pairs. Besides the results for detection via MCT array (blue) and CPU (red), we calculated data points for an additional averaging of five adjacent CPU data points (green,

#199085 - $15.00 USD Received 7 Oct 2013; revised 11 Nov 2013; accepted 11 Nov 2013; published 5 Dec 2013

confer area confined by vertical lines in the inset of Fig. 4), compensating for the unequal spectral coverage. The corresponding standard deviations are listed in Table 1. The additional binning reduces the standard deviation of CPU detection by approximately 13 %. Nevertheless, with respect to MCT detection, the corresponding distributions are broadened by a factor 2.6 in the measurement with no sample and by a factor 2.1 in the measurement with sample and pump-interaction, respectively. The observed excess noise using CPU is in good agreement with the finding that the MIR OPA can run significantly more stable than the fundamental 800 nm laser output itself [3]. A rough estimate of the additional noise which is transferred to the CPU transient absorption spectrum can be made by considering error propagation: thereby, the assumption that the CP is 2.4-times less stable than the MIR corresponds to the factor which was observed in the measurement with no sample. Note that these results represent the detection of absorption changes in the vicinity of the spectral maximum: up to 6000 counts per data point (2 pixel binned) per single shot are detected in the 16 bit range of the CCD camera and the integrated photodiode signals are held below 60 percent of the analog-digital-conversion range using an additional neutral density attenuator (0.3 OD) in front of the IR spectrometer. Following the assumption that the noise in the CPU approach is dominated by fluctuations of the CP, the noise level can be reduced drastically by normalization of individual CPU spectra with the spectrally integrated signal for each laser shot. The resulting standard deviations of 50000 pump-probe pairs after normalization of individual CPU spectra can be seen from Table 1, corresponding distributions are shown in Fig. 5 (black and gray). After correction for intensity fluctuations, the standard deviation obtained using CPU with an additional binning of five adjacent data points even falls slightly below the value obtained using direct MCT detection. The CCD camera is used far from its saturation, so that increasing the CPU signal, either by employing a higher intensity of the CP or the MIR beam, should further reduce remaining noise contributions. Note that normalizing the probe spectra reduces the noise, but will affect the absolute value of transient absorption changes because of different spectrally integrated probe signals in the presence or absence of a pump pulse. However, this scaling can be accounted for in the data evaluation.

Table 1. Standard deviation of 50000 consecutively measured pump-probe pairs at 2039 $cm^{-1}$ corresponding to the histograms shown in Fig. 5.

| measurement conditions | no sample | sample and pump-interaction |
|---|---|---|
| MCT | 2.7 mOD | 3.7 mOD |
| CPU | 8.1 mOD | 8.9 mOD |
| CPU - 5 data points binned | 7.1 mOD | 7.7 mOD |
| CPU - spectra normalized | 4.7 mOD | 5.5 mOD |
| CPU - 5 data points binned - spectra normalized | 2.5 mOD | 3.1 mOD |

Providing a measure for the time which is necessary to obtain a certain noise level in the detection of absorption-change signals, Fig. 6 displays log-log-plots of the absorption-change standard error as a function of the considered, consecutively measured, pump-probe pairs for baseline-detection (left panel, no sample) and the detection of absorption changes (right panel, sample and pump-interaction). We want to emphasize that each data point reflects the evaluated standard error after a particular number of pump-probe pairs, rather than just an extrapolation of the standard error based on the standard deviation of 50000 pump-probe pairs. The MCT detection exhibits considerably lower noise levels than detection via CPU. For instance, to reach

#199085 - $15.00 USD Received 7 Oct 2013; revised 11 Nov 2013; accepted 11 Nov 2013; published 5 Dec 2013

a level of 50 μOD in the measurement with sample and pump-interaction using MCT detection, only 5200 pump-probe pairs are required, which is in good agreement with values reported in the literature [13]. In comparison, 31700 pump-probe pairs acquired using CPU provide the same data quality. With an additional binning of five data points, this value is reduced to 23100. Other noise levels can analogously be evaluated by looking at the intersections of the measured data with horizontal lines representing the desired data quality. Corresponding to the consequences on the standard deviation (confer Table 1), normalization of CPU spectra with the spectrally integrated signal leads to a reduction of the number of pump-probe pairs required for a certain noise level, so that 12600 pump-probe pairs are needed in CPU with normalized spectra to reach 50 μOD in the measurement with sample and pump-interaction. For CPU detection with an additional binning of five adjacent data points, the same noise level is reached after 4000 pump-probe pairs.

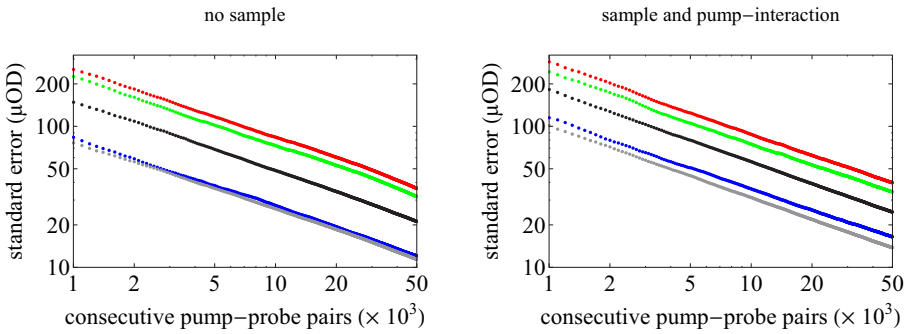


Fig. 6. Absorption-change noise level of a single data point at 2039 $cm^{-1}$ when detecting $\Delta Abs = 0$ (left panel, no sample) and $\Delta Abs \approx 2$ mOD (right panel, sample and pump-interaction): standard error versus the number of considered background-corrected pump-probe pairs using MCT detection (blue), CPU (red) or CPU with an additional binning of five adjacent data points (green). Noise levels resulting after normalization of individual spectra with their integrated spectral intensity are shown for CPU detection (black) and CPU detection with an additional binning of five adjacent data points (gray). Note that these graphs have a double-logarithmic scale.

As reported elsewhere [35, 38], and confirmed in a separate measurement with our setup, dark noise contributions of the detectors are small compared to laser shot-to-shot fluctuations and are neglected in the following analysis of individual noise contributions. In Fig. 7, the absorption-change standard error is plotted versus the spectral position. With this, the influence of both the different signal strengths (confer CPU spectra in the background: respective CCD counts are depicted on the right vertical axis) and the sample under pump-interaction can be dissected. Within the FWHM of the spectrum, both detection methods exhibit almost constant baseline noise levels. Note that with MCT detection (blue), only the higher energetic part of the MIR spectrum was probed. In the measurement with sample and pump-interaction, small deviations arise around 2060 $cm^{-1}$. This can be attributed to the reduced spectral intensity due to the absorption of the parent complex ($\approx$ 0.43 OD at 2060 $cm^{-1}$) and the pump-induced absorption changes. In the other regions, no deviations between both measurement runs emerge. Consequently we can infer that no additional noise is added by the liquid sample film.

#199085 - $15.00 USD Received 7 Oct 2013; revised 11 Nov 2013; accepted 11 Nov 2013; published 5 Dec 2013

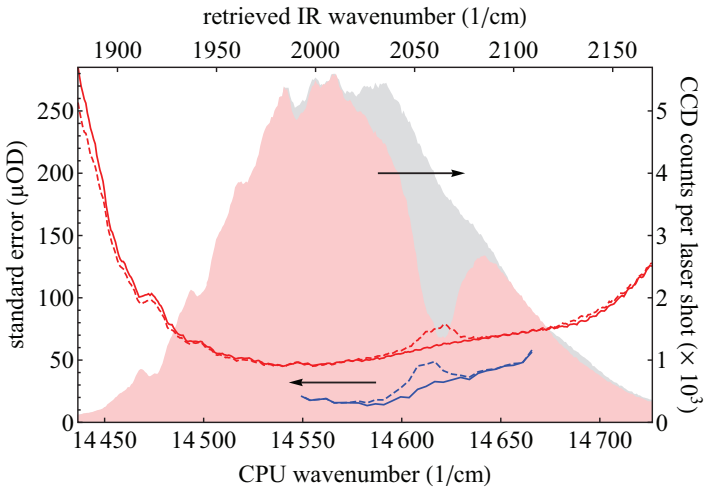


Fig. 7. Absorption-change standard error as a function of the spectral position: data obtained via MCT (blue) and CPU detection (red) after averaging 25000 consecutive pump-probe pairs when detecting $\Delta\mathrm{Abs} = 0$ (solid lines, no sample) and a molecular signal (dashed lines, sample and pump-interaction, confer transient absorption spectra in Fig. 4); the CPU curves with binned data points or with normalized spectra, or with both, are not shown for clarity; the corresponding CPU spectra, with sample (light red) and without sample (light gray), are shown in the background.

In [35], Cheatum and coworkers found an improved signal-to-noise ratio when measuring the average of 115 2D IR spectra using CMOS array detection after upconversion instead of direct MIR detection. The study differs from ours by the facts that no chirped NIR pulse was used for upconversion, that a different visible detector was employed, and that MIR signals were recorded with only a single MCT pixel. The measurement times to record 2D IR spectra were shortened by a factor 60 using CMOS array detection, and in this way, additional noise contributions originating from long-term laser drifts are reduced. Our results also confirm that noise levels comparable to direct MCT measurements can be achieved when the detection is done after upconversion. We want to emphasize that in our comparative study all reported noise levels result from the same number of laser shots under unaltered measurement conditions representing single data points.

## 4. CPU phase-matching characteristics

The alignment of the CPU crystal is normally optimized to upconvert a given MIR spectrum as effectively as possible. However, promising possibilities also arise when the crystal's phase-matching is set differently. Imagine a situation where the features of interest are spectrally far apart and merely covered by the edges of the CPU spectrum. Whereas the central part of a bell-shaped spectrum thereby potentially saturates the detector, the spectral edges suffer from a low number of counts resulting in aggravated noise levels. In the following, we demonstrate the simultaneous detection of absorption-change signals separated by more than 200 $\mathrm{cm}^{-1}$ using a modified CPU spectrum, of which the central part is selectively lowered by means of a changed phase-matching configuration. For this purpose, we use a MIR spectrum which is centered at 1940 $\mathrm{cm}^{-1}$ (Fig. 8(a)), covering absorption bands of $Co_4(CO)_{12}$ at 1860 and 2060 $\mathrm{cm}^{-1}$ (confer MIR absorption spectrum in Fig. 8(b), recorded with JASCO FT/IR-4100 spectrometer).

#199085 - $15.00 USD Received 7 Oct 2013; revised 11 Nov 2013; accepted 11 Nov 2013; published 5 Dec 2013

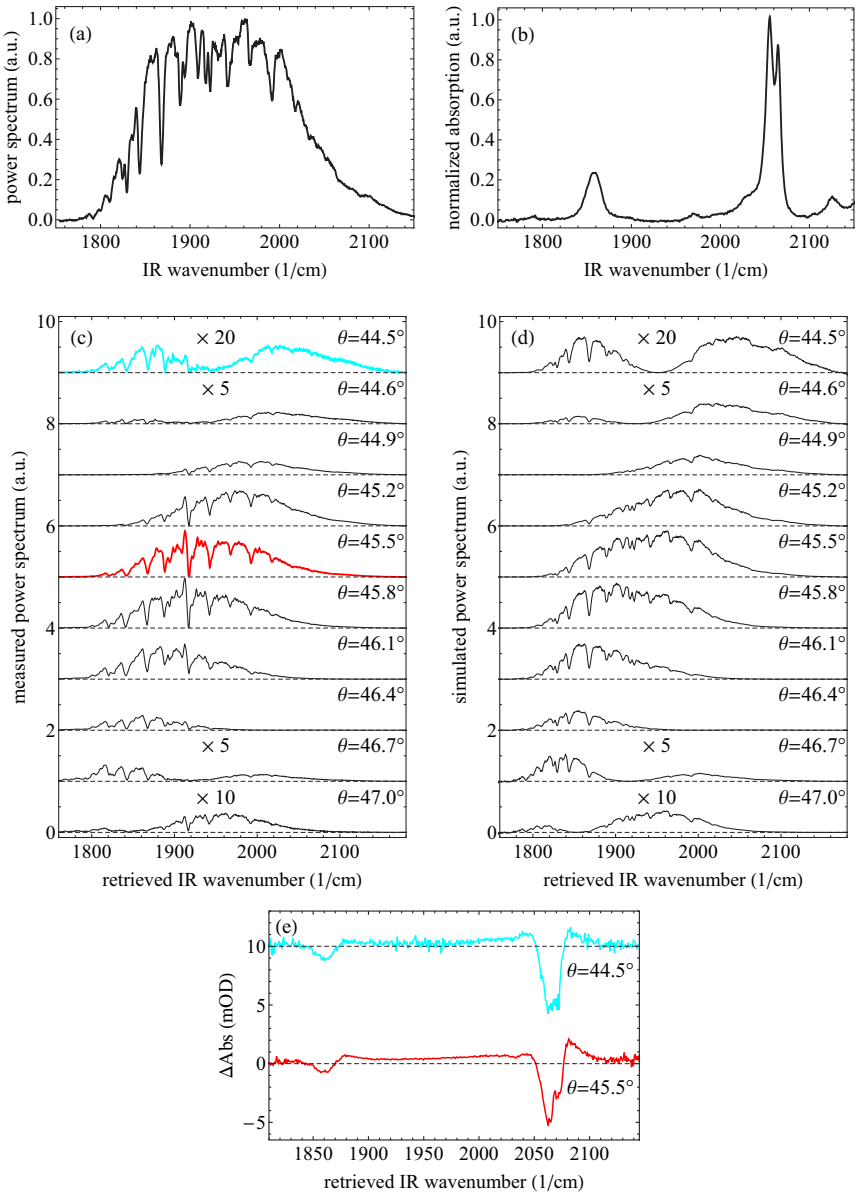


Fig. 8. (a) MIR spectrum obtained with a single MCT pixel by scanning the central IR spectrometer wavelength in steps of 1 nm (centered at 1940 $cm^{-1}$, FWHM 185 $cm^{-1}$, 100 laser shots averaged per step). (b) MIR absorption spectrum of $Co_4(CO)_{12}$ dissolved in $CH_2Cl_2$. (c) Measured CPU spectra at different phase-matching angles. (d) Simulated CPU spectra at different phase-matching angles. (e) Transient absorption spectra of $Co_4(CO)_{12}$ at 6 ps pump-probe delay: data obtained by averaging 100000 consecutive pump-probe pairs at CPU phase-matching angles of $\theta = 45.5°$ (red) and $\theta = 44.5°$ (cyan, 10 mOD vertical offset).

#199085 - $15.00 USD Received 7 Oct 2013; revised 11 Nov 2013; accepted 11 Nov 2013; published 5 Dec 2013

The uniaxial MgO(5%):$LiNbO_3$ crystal is suited for sum-frequency mixing of 800 nm pulses with MIR pulses around 5 μm. Usually, a specific crystal cut angle $\theta$ is chosen with respect to the spectral range of interest. Optimized for MIR pulses centered at 5 μm, the actual cut angle of our crystal is $\theta = 45.4^\circ$. Nevertheless, we are able to mimic different configurations by rotating the crystal and thereby changing the angle $\alpha$ between the incident beams and the optical axis of the crystal. Thereby the actual change of the angle between the optical axis of the crystal and the propagation direction of the beams within the crystal ($\Delta\theta$) is determined by Snell's law. Resulting CPU spectra for different crystal settings are shown in Fig. 8(c). In this series, the crystal was rotated in steps of $\Delta\alpha = 0.7^\circ$ in both directions starting at the optimal phase-matching configuration (red, $\theta = 45.5^\circ$). Note that due to the spectral position of the given IR spectrum (central wavelength of 5.2 μm instead of 5.0 μm), the latter configuration requires an angular offset of $\Delta\theta = +0.1^\circ$ with respect to the crystals cut angle. We observe that for increasing variations from the optimal setting, the center of the CPU spectrum is shifted either to the lower or to the higher energetic regime. Aberrant from this trend, larger angles lead to the formation of double peak spectra, revealing counts primarily on the edge of the initial MIR spectrum. At $\theta = 44.5^\circ$ an almost symmetric case is reached. Due to the reduced efficiency of upconversion, the maximum single-shot intensity is thereby reduced by approximately a factor of 20 with respect to the optimum case, whereas the intensity at the spectral edges remains almost unchanged.

To support our experimental findings, we calculated the sum-frequency-generation efficiencies of a 450 μm thick MgO(5%):$LiNbO_3$ crystal for different phase-matching angles when mixing MIR light with monochromatic 800 nm light in a type I SFG arrangement. At this, we follow the derivations from [39] applying the Sellmeier coefficients from [40]. Using the wavevector mismatch

$$\Delta k = k_{\mathrm{NIR}} + k_{\mathrm{MIR}} - k_{\mathrm{SFG}} \ , \tag{1}$$

the intensity of the sum-frequency signal is given by

$$I_{\mathrm{SFG}} = \frac{8 d_{\mathrm{eff}}^2 \omega_{\mathrm{SFG}}^2 I_{\mathrm{NIR}} I_{\mathrm{MIR}}}{n_{\mathrm{NIR}} n_{\mathrm{MIR}} n_{\mathrm{SFG}} \varepsilon_0 c^2} L^2 sinc^2\left(\frac{\Delta k L}{2}\right) \ , \tag{2}$$

where $d_{\mathrm{eff}}$ is the nonlinear efficiency parameter, $\omega_{\mathrm{SFG}}$ the carrier angular frequency of the upconverted field, $I_{\mathrm{NIR}}$ and $I_{\mathrm{MIR}}$ the intensities of the incident fields, $n_{\mathrm{NIR}}$, $n_{\mathrm{MIR}}$ and $n_{\mathrm{SFG}}$ the respective refractive indices, $\varepsilon_0$ the vacuum permittivity, $c$ the speed of light, and $L$ the crystal thickness. Consequently, the free parameters are $\lambda_{\mathrm{MIR}}$ and the phase-matching angle $\theta$. CPU spectra after upconversion under different phase-matching conditions can be simulated by multiplying the MIR spectrum from Fig. 8(a) by the corresponding efficiency curves. Fig. 8(d) shows simulated CPU spectra under phase-matching angles corresponding to the series which was conducted experimentally (confer Fig. 8(c)). Taking account of the different optical MIR paths resulting in different manifestations of water vapor absorption lines, the simulations are in excellent agreement with measured spectra.

The CPU intensities in our particular setup are in general too low to saturate the CCD detector. Nevertheless, we can scrutinize different phase-matching settings when detecting absorption changes. Therefore, we recorded transient absorption spectra of 100000 pump-probe pairs using CPU spectra at $\theta = 45.5^\circ$ (red) or $\theta = 44.5^\circ$ (cyan), respectively. Both transient absorption spectra show analogue results, revealing the ground-state-bleach signals of the parent complex at 1860 and 2060 $cm^{-1}$ (Fig. 8(e)). Whereas the noise level in the inner part of the detection range is significantly degraded under detection at $\theta = 44.5^\circ$, the noise level at the spectral edges is comparable. Such a scenario could be beneficial when saturation of the detector in regions where the MIR is most intense has to be circumvented.

#199085 - $15.00 USD Received 7 Oct 2013; revised 11 Nov 2013; accepted 11 Nov 2013; published 5 Dec 2013

## 5. Conclusion

Overall, this comparative study confirms that CPU constitutes a powerful alternative to direct multichannel MCT detection. We verified the accordance between MIR spectra before and after upconversion to the visible regime, thereby observing only negligible changes in the spectral shape and the spectral bandwidth. In an exemplarily chosen UV-pump/MIR-probe experiment in the liquid phase, we examined the individual advantages and disadvantages of both methods when detecting weak absorption-change signals on the order of a few mOD. Although intensity fluctuations of the chirped beam are transferred to MIR spectra in the additional nonlinear upconversion process, CPU spectra after normalization with the integrated spectral intensity showed noise levels similar to direct MCT detection. Moreover, CPU scores with the high pixel numbers of the easy-to-handle and more cost-effective CCD detectors. In most cases, the CPU detection bandwidth as a limiting factor can almost be excluded. Future applications of CPU might also benefit from the possibility to adapt the shape of the upconverted spectrum by using different phase-matching configurations, thereby avoiding too high signals in very intense spectral regions.

## Acknowledgments

The authors thank Tobias Brixner, Florian Kanal, Jarno Riefer, and Florian Lessing for fruitful discussions and their help. Furthermore, we are very grateful to Manuel Joffre for stimulating input on the topic of chirped-pulse upconversion. This publication was funded by the German Research Foundation (DFG) and the University of Wuerzburg in the funding program Open Access Publishing. We further acknowledge the DFG for financial support within the Emmy-Noether program and within the Research Unit “Light-induced Dynamics in Molecular Aggregates” (FOR 1809).